This is a repository copy of *Siderite concretions from nonmarine shales (Westphalian A) of the Pennines, England: Controls on their growth and composition* .

White Rose Research Online URL for this paper:
http://eprints.whiterose.ac.uk/399/

Article:

SIDERITE CONCRETIONS FROM NONMARINE SHALES (WESTPHALIAN A) OF THE PENNINES, ENGLAND: CONTROLS ON THEIR GROWTH AND COMPOSITION

Q.J. FISHER[1], R. RAISWELL[1], AND J.D. MARSHALL[2]

[1] *Department of Earth Sciences, University of Leeds, Leeds LS2 9JT, UK*
[2] *Department of Earth Sciences, Liverpool University, L69 3BX, UK*

ABSTRACT: Back-scattered electron microscopy has been used to examine the microstructure of nonmarine-shale-hosted siderite concretions. The concretions are composed of 50–100 μm, zoned crystallites, which exhibit no noticeable center-to-edge variation within any individual concretion. This indicates that siderite crystallites nucleated at virtually the same time across the entire concretion and that the concretions did not grow by radial addition of siderite layers around a central nucleus. Further siderite precipitation took place by crystal growth onto the nuclei. The total proportion of siderite in any part of the concretion bears no simple relationship to the porosity of the enclosing shale at the time of precipitation, and growth by passive precipitation in pore space is unlikely. Integration of microprobe data with bulk mineral-chemical and stable-isotope data suggests that the siderite crystallites are composed of an Fe-Mn-rich end member with a $\delta^{13}C$ value of $\sim +10‰$ and a Mg-Ca-rich end member with a $\delta^{13}C$ value of $\sim 0‰$ to $-5‰$. The mineral-chemical and stable-isotope compositions of these concretions resulted from microbially mediated processes operating close (< 10 m) to the sediment–water interface, during methanogenesis. Methanogenesis can generate low-$\delta^{13}C$ as well as high-$\delta^{13}C$ carbonate cements, hence deep-burial diagenetic reactions, such as decarboxylation of organic matter, need not be invoked to generate solutes for siderite precipitation.

INTRODUCTION

Intensive research over the last three decades has provided compelling evidence that most, if not all, mudrock-hosted carbonate concretions began to form as a product of microbially mediated reactions, very similar to those that occur close to the sediment–water interface in present-day sediments (e.g., Raiswell 1971; Curtis et al. 1975; Curtis et al. 1986; Coleman and Raiswell 1993). The results of geochemical and stable-isotope investigations of concretions (e.g., Irwin et al. 1977) have been integrated with studies of pore-water composition (e.g., Rosenfeld and Silverman 1959; Claypool and Kaplan 1974; Froelich et al. 1979) and the bulk mineralogy of fine-grained sediments (e.g., Hower et al. 1976) to obtain both a general model for the growth of concretions (e.g., Irwin et al. 1977; Curtis et al. 1986) and a zonal scheme for the diagenetic evolution of organic-rich mudrocks (e.g., Curtis 1977).

Until recently, the most widely accepted model for the growth of mudstone-hosted concretions requires that growth began close to the sediment–water interface and occurred from the center outwards by the lateral accretion of successive generations of carbonate cement. It is frequently assumed that the carbonate passively replaced pore water. Consequently, the proportion of cement is often taken to be equivalent to the porosity of the host sediment at the time of mineral precipitation (Lippmann 1955; Seibold 1962; Raiswell 1971; Oertel and Curtis 1972; Gautier and Claypool 1984; Curtis et al. 1986). These porosity estimates have been combined with shale compaction models, such as those of Baldwin and Butler (1985), to derive an estimate for the depth of cement precipitation (Curtis et al. 1986). Variations in the amount of carbonate and its mineral-chemical and isotopic composition between and across individual concretions are often remarkably consistent with this growth model (e.g., Raiswell 1971; Irwin et al. 1977; Curtis et al. 1986).

The siderite concretions from the nonmarine shales of the Hepworth

quarries, near Penistone, South Yorkshire, England, have been widely studied (e.g., Oertel and Curtis 1972; Pearson 1973, 1974a, 1974b, 1977, 1979, 1985; Curtis et al. 1975; Curtis et al. 1986; Curtis and Coleman 1986) and offer one of the best examples of bulk chemical, mineral-chemical, and stable-isotope data that are consistent with the growth model outlined above. The concretions are usually present within gray shales and mudrocks as oblate nodules oriented parallel to bedding. Generally ranging in diameter between ~ 5 and 40 cm, they are present in isolation or within laterally persistent bands; sideritic sheets are also present that are laterally continuous over the whole length of quarry faces (> 100 m). The deformation of bedding around the concretions provides unequivocal evidence that they began to form during shallow burial.

The amount of siderite within the concretions usually decreases from a maximum of $\sim 70\%$ in their center down to as low as 5% at their margins (Curtis et al. 1986). This is equivalent to precipitation at burial depths of several meters and several kilometers, respectively, assuming that the amount of carbonate reflects the porosity of the host sediment at the time of cement precipitation. The siderite at the centers of the concretions is frequently Mn-rich and enriched in ^{13}C; Mn concentrations as high as 14 mole % and $\delta^{13}C$ values as high as $+10‰$ have been reported (Curtis et al. 1986). The siderite from the margins of concretions tends to be Mg-Ca-rich and depleted in ^{13}C; Mg concentrations of up to 19 mole %, Ca concentrations of as high as 16 mole %, and $\delta^{13}C$ values as low as $-3‰$ have been reported (Pearson 1985; Curtis et al. 1986). These results were interpreted as showing that the Mn-rich siderite, at the centers of concretions, precipitated soon after sediment deposition as a product of microbially mediated iron reduction, manganese reduction, and methanogenesis. The increase in the Mg-Ca content and decrease in $\delta^{13}C$ values was believed to have occurred because clay-mineral transformation and thermal decarboxylation of organic matter became important sources of solutes for siderite precipitation during deeper burial (Pearson 1979, 1985; Curtis and Coleman 1986).

The published results outlined above appear to suggest that concretions have the potential to record changes in pore-water chemistry throughout shale burial. However, this model for concretion growth is based on the assumption that the amount of carbonate within any part of the concretion reflects the porosity of the sediment at the time of cement precipitation, yet this has never been supported by microstructural data. This is an important omission, especially when recent work on other groups of concretions suggests that carbonate may not always precipitate by passive infill of porosity (e.g., Mozley 1989, 1996; Feistner 1989). Furthermore, Mozley (1996) noted that most of the evidence typically used to support the passive-infill model can be explained by other modes of growth, and concluded that the passive-infill mechanism may be the exception rather than the rule, at least for concretions in marine mudrocks.

The aim of this paper is to present new microstructural and microchemical data, obtained using back-scattered electron microscopy (BSEM) and electron microprobe analysis (EMPA), which show that some aspects of the previous models for the growth of the Hepworth siderite concretions are incorrect. These data are integrated with published results from modern sediment studies to show that the stable-isotope and geochemical variations across and between concretions can be explained in terms of processes that operate close to the sediment–water interface rather than pore-water evolution during sediment burial. In broader terms, this work suggests that
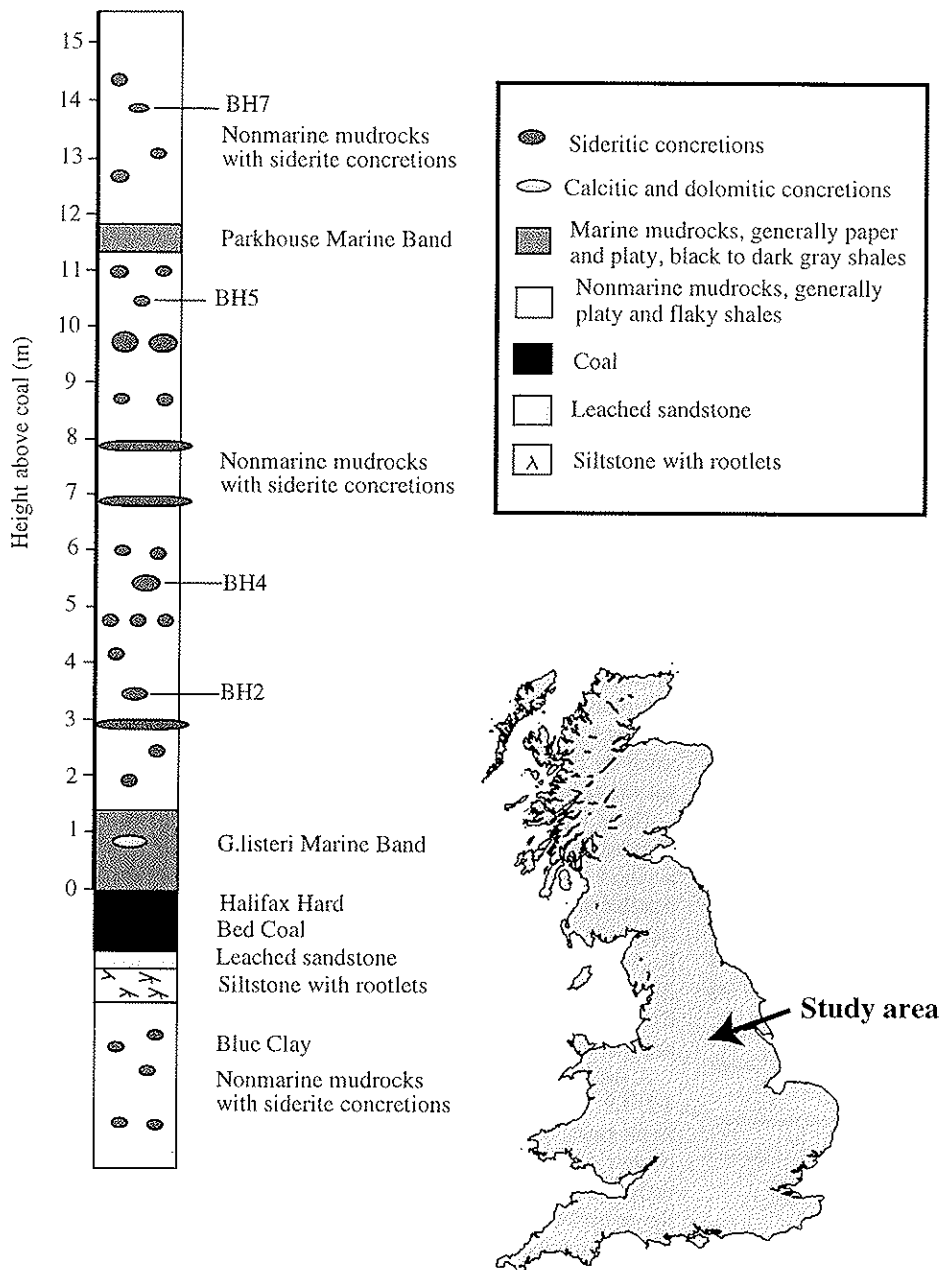
zonal schemes for shale diagenesis that have been based on integration of results from studies of concretions and modern pore waters should be re-evaluated.

STUDY AREA

Material for this study was collected from the Westphalian A, Bullhouse Quarry (UK National grid reference SE 209023), which is owned by Hepworth Industrial Building Products Ltd.

The lower part of the sequence (Fig. 1) is composed of mudrocks, rootlet-rich siltstones, and bleached sandstones that probably represent nonmarine sediments that were emergent above the water table and chemically modified by eogenetic processes (Curtis and Coleman 1986). The sediments were subsequently buried beneath a developing peat swamp (later to become the Halifax Hard Bed Coal). However, chemical leaching probably continued because of recharge of slightly acidic, anoxic waters within the phreatic zone beneath the peat swamp (Curtis and Coleman 1986).

Directly overlying the Halifax Hard Bed Coal is the Alton (G. listeri) Marine Band. This comprises ~ 1 m of dark gray and black pyritiferous mudrocks containing a low-diversity, but highly abundant, marine fauna.

The rest of the succession (up to 20 m) is composed predominantly of dark–medium gray mudrocks; these contain abundant sideritic concretions and a limited fauna thought to indicate that the sediments were deposited in a fresh to brackish-water environment (Calver 1968a). This sequence of nonmarine mudrocks is broken by a thin dark-gray shale that probably represents the Parkhouse Marine Band (cf. Calver 1968b).

ANALYTICAL METHODS

Four concretions were sampled from the Bullhouse Quarry. BH2 and BH4 were collected from ~ 2 m and ~ 4 m above the Halifax Hard Bed
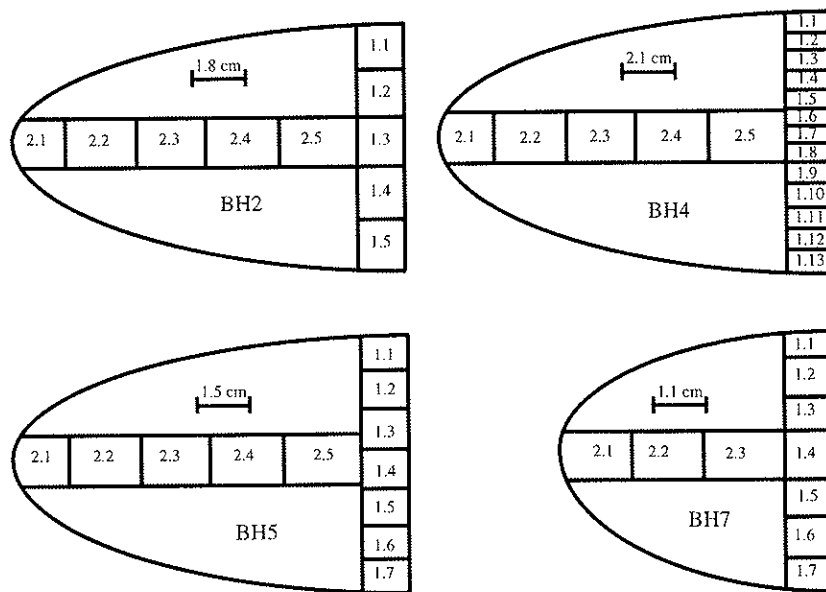
FIG. 2.—Position of the subsamples in the central slice of each concretion collected.

Coal, respectively, BH5 was collected from ~ 1 m below the Parkhouse Marine Band, and BH7 was collected from ~ 2 m above this horizon. A 20 mm thick slice was cut through the center of each concretion and was subsectioned (Fig. 2). X-ray diffraction (XRD) analysis showed the samples to be composed mainly of siderite, quartz, kaolin, mica, and chlorite.

Around 500 mg of each powdered sample were accurately weighed, and then the siderite was dissolved by reaction with 10% HCl for 24 hours at room temperature. The solutions were analyzed by ICP-AES for P, Al, Fe, Mg, Ca, and Mn. Carbonate-free shales from around each concretion were leached in the same manner, and the leachates were analyzed for both major and minor elements, allowing a correction for silicate dissolution within the concretion samples to be made. The ICP-AES was calibrated using standard solutions made in the same HCl matrix as the diluted leachates. The residues were analyzed for organic carbon using a Carlo Erba 1106 elemental analyzer. Unleached samples were also analyzed for total carbon using the elemental analyzer, and the content of inorganic carbon was calculated by subtracting organic carbon from total carbon.

The ICP-AES raw data were corrected, using the methods described in Pearson (1974a), for apatite dissolution (all phosphorus in solution was assumed to be from dissolved francolite), blank composition, and silicate dissolution in order to determine the bulk chemical composition of the siderite in each subsample. For the latter correction, it was assumed that Fe, Mn, Ca, and Mg were leached from silicates in direct proportion to the Al in solution and that this proportion was exactly the same in the leachates from the concretion subsamples as in the leachate from the carbonate-free shale surrounding the concretion.

A selected number of subsamples (BH2 1.2, 1.4, 1.5, 2.2, 2.5; BH4 1.1, 1.2, 1.9 1.10, 1.13, 2.5) were chosen for stable carbon isotopic analysis. Approximately 50 mg of each carbonate powder was leached with 10% chlorax solution overnight, in order to oxidize labile organic matter. After drying, the remaining organic matter was removed using a Bio-Rad E2000 low-temperature plasma asher. Approximately 3–5 mg of each subsample was then reacted with 2 ml of 100% orthophosphoric acid under high vacuum (typically $< 5 \times 10^{-5}$ atm), at 50°C, until all signs of reaction had ceased (generally ~ 2 weeks). Purified CO_2 samples were analyzed using an automated VG Isogas SIRA 12 triple-collector mass spectrometer by comparison with an internal standard calibrated to the NBS19 international standard. The reproducibility of the stable carbon isotope analyses was measured by conducting up to three repeat analyses of each sample (Table 1). Oxygen isotopes were also measured, but these had poor reproducibility and so are not presented. In addition, interpretation of oxygen-isotope data from siderite concretions is often problematic, possibly because of the influence of microbial action on isotopic fractionation (Mortimer and Coleman 1997).

Samples from across the BH2, BH4, BH5, and BH7 concretions were polished and carbon coated, and their microstructure was examined using a CAMSCAN Series 4 scanning electron microscope (SEM) equipped with a Link Systems 1055s energy-dispersive X-ray spectrometry (EDX) system. Quantitative microchemical data were obtained from each sample using a Cameca SX-50 electron microprobe. Iron was calibrated using hematite, Ca and Mg using dolomite, and Mn using rhodonite standards. Since two

TABLE 1.—Stable-isotope data from selected subsamples of the BH2 and BH4 sideritic concretions.

Sample Number	$\delta^{13}C$ PDB	Mean	σ
BH2 1.2	4.23 4.26 4.25	4.24	0.01
BH2 1.4	3.33 3.39 3.43	3.39	0.05
BH2 1.5	1.88 1.91 1.84	1.88	0.03
BH2 2.2	0.89 0.56 0.72	0.73	0.16
BH2 2.5	3.67 3.71 3.54	3.64	0.09
BH4 1.1	4.86 4.87 4.54	4.76	0.19
BH4 1.2	5.07 4.79	4.93	0.20
BH4 1.9	8.81 8.58 8.20	8.53	0.31
BH4 1.10	8.95 8.82	8.89	0.09
BH4 1.13	6.06 6.02 6.09	6.06	0.04
BH4 2.5	6.44 6.50	6.47	0.04

TABLE 2.—*Bulk chemistry of the siderite in the BH2, BH4, BH5, and BH7 concretion subsamples (see Fig. 2).*

Sample Number	Mole Fraction				P (mg/g)	CO_2 (A) (wt.%)	CO_2(B) (wt.%)	Org.—C (wt.%)	Siderite (wt.%)
	Fe	Mg	Ca	Mn					
BH2									
1.1	0.785	0.133	0.048	0.034	10.3	28.4	29.0	3.8	72.0
1.2	0.796	0.119	0.048	0.036	4.7	33.7	33.0	4.3	85.3
1.3	0.789	0.127	0.049	0.035	6.6	32.9	32.5	4.1	83.3
1.4	0.780	0.141	0.048	0.032	11.7	29.7	29.2	4.0	75.0
1.5	0.761	0.152	0.053	0.034	9.2	22.1	21.8	2.8	55.7
2.1	0.771	0.141	0.051	0.035	2.4	20.0	19.5	2.4	50.4
2.2	0.764	0.155	0.050	0.031	6.5	24.6	25.3	2.8	61.8
2.3	0.774	0.141	0.053	0.032	6.5	30.9	30.9	3.5	78.0
2.4	0.789	0.130	0.047	0.034	5.9	31.6	31.7	4.2	79.0
2.5	0.799	0.120	0.045	0.036	6.1	31.8	32.3	4.2	80.7
BH4									
1.1	0.753	0.148	0.059	0.038	4.2	8.9	7.4	2.9	22.5
1.2	0.788	0.135	0.045	0.031	20.9	22.4	22.2	3.5	57.3
1.3	0.792	0.128	0.049	0.030	16.0	24.0	23.3	3.8	61.2
1.4	0.805	0.127	0.038	0.030	27.4	23.5	24.2	4.0	60.5
1.5	0.807	0.122	0.040	0.031	12.1	28.8	27.8	4.0	73.3
1.6	0.809	0.122	0.038	0.030	20.7	26.4	26.2	4.6	67.6
1.7	0.813	0.115	0.041	0.031	6.7	31.6	31.5	3.9	80.3
1.8	0.848	0.081	0.032	0.039	5.7	32.7	32.6	4.5	83.9
1.9	0.871	0.053	0.030	0.047	6.6	33.5	33.0	5.4	86.7
1.10	0.895	0.036	0.015	0.054	8.7	33.0	32.8	6.2	86.2
1.11	0.867	0.061	0.029	0.044	4.1	34.2	34.1	5.4	88.3
1.12	0.835	0.092	0.036	0.036	4.0	33.6	33.1	4.6	86.0
1.13	0.790	0.130	0.046	0.034	4.7	18.8	18.4	2.9	47.5
2.1	0.801	0.117	0.045	0.037	2.6	20.6	18.5	2.9	52.3
2.2	0.807	0.116	0.044	0.033	6.7	24.8	24.6	2.7	63.0
2.3	0.816	0.108	0.043	0.034	15.8	26.1	26.4	3.5	66.9
2.4	0.827	0.102	0.037	0.034	15.4	28.6	28.7	3.5	73.3
2.5	0.833	0.096	0.035	0.036	9.1	30.4	30.2	3.9	77.9
BH5									
1.1	0.834	0.111	0.046	0.008	5.0	24.5	23.3	2.2	62.3
1.2	0.824	0.121	0.048	0.007	11.3	25.8	25.9	2.0	65.7
1.3	0.838	0.109	0.045	0.008	4.4	28.9	28.5	2.2	73.4
1.4	0.862	0.087	0.041	0.009	3.2	29.8	30.0	2.4	76.3
1.5	0.841	0.106	0.045	0.008	3.4	30.8	29.5	2.1	78.3
1.6	0.840	0.107	0.045	0.008	3.1	30.4	29.1	2.3	77.5
1.7	0.825	0.120	0.048	0.007	4.8	23.6	22.1	1.6	59.8
2.1	0.827	0.114	0.050	0.009	2.2	21.6	20.2	1.4	54.9
2.2	0.831	0.115	0.047	0.008	3.2	28.8	27.7	1.9	73.2
2.3	0.835	0.110	0.047	0.008	3.3	30.6	29.2	2.1	77.6
2.4	0.845	0.106	0.042	0.008	3.2	26.0	25.9	2.3	66.3
2.5	0.855	0.096	0.041	0.008	3.1	26.6	27.4	2.2	68.8
BH7									
1.1	0.779	0.147	0.058	0.017	1.4	9.1	9.8	2.4	22.9
1.2	0.771	0.153	0.062	0.014	9.1	24.3	24.8	3.0	60.9
1.3	0.768	0.151	0.069	0.012	19.7	25.6	25.1	4.0	64.9
1.4	0.780	0.131	0.078	0.011	25.2	25.6	25.4	4.5	65.4
1.5	0.803	0.125	0.060	0.012	14.4	29.3	29.6	4.6	74.6
1.6	0.799	0.125	0.063	0.013	12.2	29.3	29.1	4.2	74.4
1.7	0.781	0.148	0.060	0.012	7.9	15.9	15.5	3.2	40.2
2.1	0.782	0.148	0.052	0.017	2.7	17.0	17.3	3.0	42.8
2.2	0.797	0.144	0.046	0.013	14.7	17.8	18.0	3.9	45.2
2.3	0.810	0.134	0.042	0.014	16.0	25.5	25.5	4.6	65.0

CO_2(A) is the amount of CO_2 within the siderite, calculated on a whole-rock basis from the ICP-AES raw data. CO_2(B) is the amount of CO_2 within the siderite, calculated on a whole rock basis from elemental analyzer results. Org.—C is the organic-carbon content measured by elemental analyzer, and calculated as a percentage of the non carbonate material present. Siderite (wt.%) is the weight % of siderite within each subsample calculated from the ICP-AES data.

of the standards were non-carbonate, the accuracy of absolute elemental concentrations will have been slightly reduced, but the pattern of relative concentrations across and between siderite crystallites are realistic. A beam size of ~ 1 μm was used, which gives an interaction volume of ~ 8 μm³; spot analyses must therefore be regarded as the average composition of this volume (E. Condliffe, personal communication 1991).

RESULTS

Bulk Chemical Compositional Trends across Concretions

The processed major- and minor-element ICP-AES data are given in Table 2. Calculation of siderite compositions required correcting the raw analytical data for both silicate and francolite dissolution, which is likely to have introduced errors. For the major elements, Fe and Mg, corrections

are generally less than 5% of the total, but samples taken from the edges of concretions contain more insoluble residue and corrections of up to 12% have been applied. The Mn data from the BH2 and BH4 concretion subsamples are corrected by less than 10%, except for the BH2 1.5 and BH4 1.1 subsamples, for which corrections of 13 and 18%, respectively, have been applied. The Mn concentrations within the siderite in the BH5 and BH7 concretions are much lower, and hence the corrections become more significant, but most are still less than 25%. The Ca correction is extremely large (up to 80%), because of the large amounts of francolite within these concretions, so the Ca content of the siderite is only approximate. It is thought that these corrections are the largest source of errors, and the total corrections applied, as outlined above, probably are a realistic upper limit for the accuracy of the siderite compositions determined by the bulk-chemical methods used in this study.
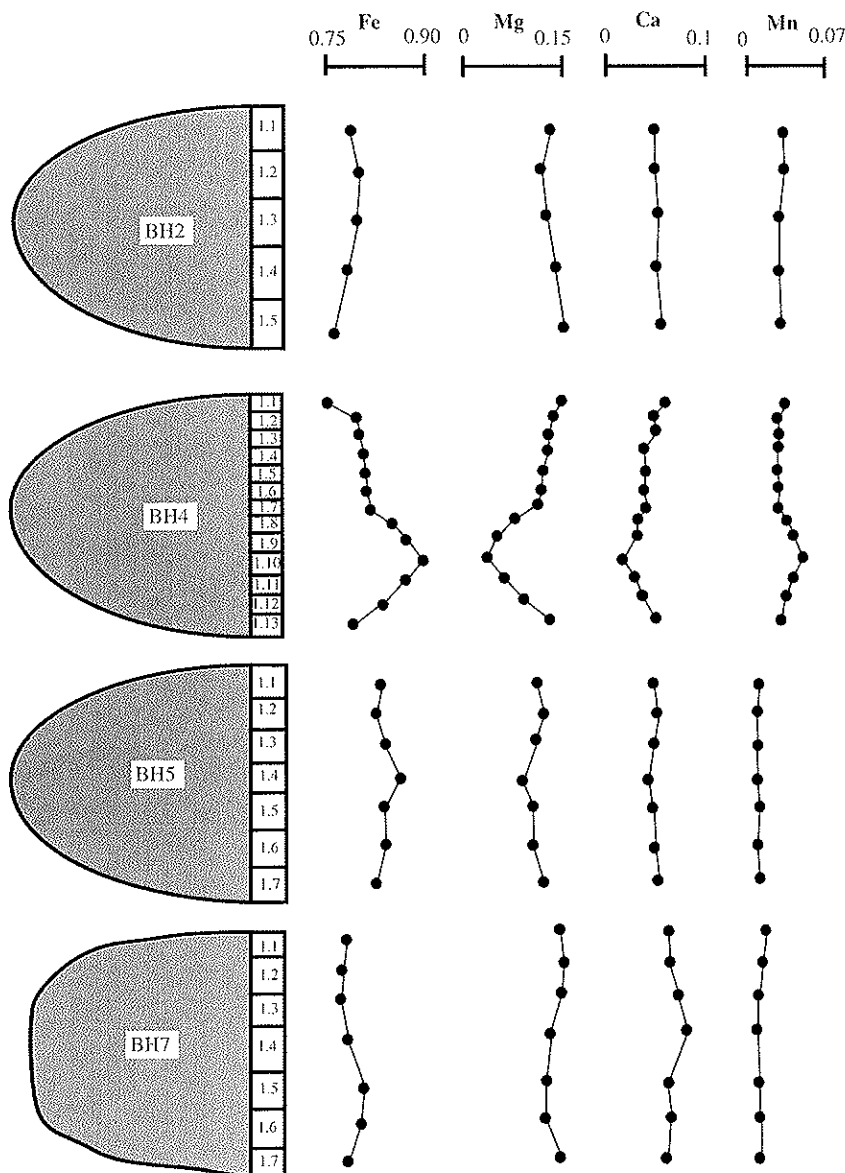
Fig. 3.—Bulk variations in the carbonate chemistry across the BH2, BH4, BH5, and BH7 sideritic concretions. All cation compositions are given as the fraction of end-member carbonate phase present.

The data on organic and inorganic carbon are included in Table 2. Repeat analysis of the internal rock standard and the MnCO$_3$ powder suggest that C analyses are accurate to ~ 7%. The quantity of carbonate measured by elemental analyzer and that calculated by recasting ICP-AES data were in close agreement (generally within 2% absolute). Organic carbon is quoted on a carbonate-free basis. The major cation compositional trends vertically through each concretions are shown in Figure 3.

All concretions show an increase in the amount of both siderite and organic matter towards approximately the same central region (Table 2). The radial decrease in the content of organic carbon may have resulted from either depositional enrichment at the site of concretionary growth or preferential loss of organic carbon from the concretion edges and host sediment during diagenesis or weathering.

In the siderite, Fe is substituted by between 4 and 15 mole % Mg, between 1.5 and 8 mole % Ca, and between 0.7 and 5.4 mole % Mn. The amount of substitution tends to vary systematically across the concretions, and the Fe/Mg and Fe/Ca ratios tend to increase concurrently with the amount of carbonate. The trend in Fe/Mg ratios is by far the most pronounced, especially in the BH4 concretion. The Mg/Mn ratio of the siderite

within the BH2, BH4, and BH5 concretions tends to decrease towards their centers. The Mn content of the siderite within the BH5 and BH7 concretions remains very low (less than 2 mole %). In the BH5 concretion, the actual Mn content remains relatively constant across the concretion. In the BH7 concretion, the Mn content of the siderite appears to decrease towards its center, but this may be an analytical artifact resulting from the large corrections applied to the Mn data from the BH7 subsamples. There is no convincing trend in the Mg/Mn ratio across the BH7 concretion. These results are in good agreement with those reported by Curtis et al. (1986).

Electron Optical Study of the Sideritic Concretions

BSEM Observations.—The siderite in the BH2 and BH4 concretions is present as 10–100 μm, lath-shaped crystallites, which are in some cases joined to form radiating aggregates (Fig. 4A). The central regions of the crystallites produce a far brighter back-scattered signal than their margins (Fig. 4A, B). EDAX analysis reveals that this is because the central regions are Mn-rich (Mg-poor) and the margins are Mg-Ca-rich (Mn-poor). The transition between the Mn-rich and Mg-rich siderite is gradual (Fig. 4A,
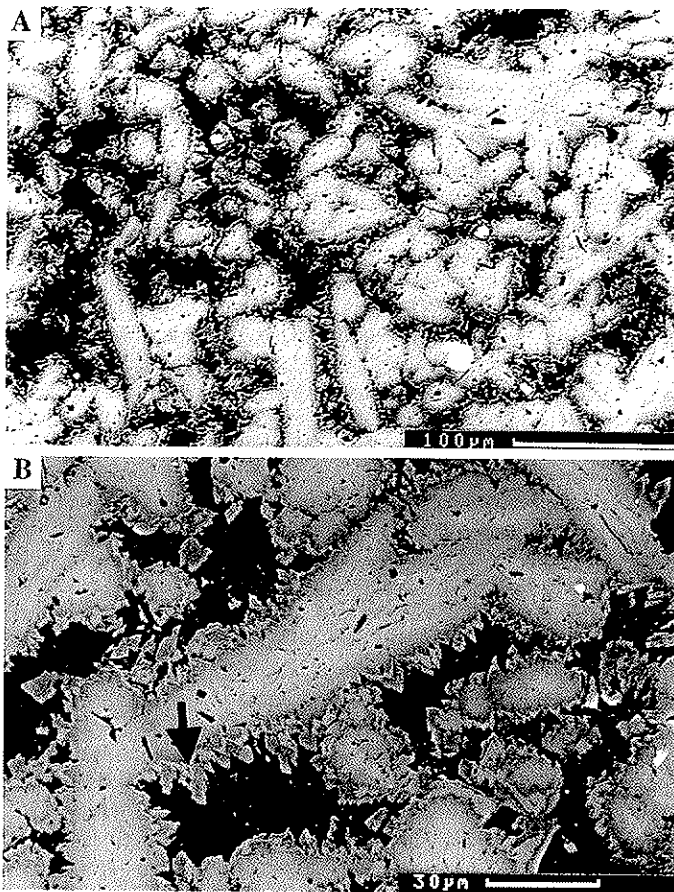
FIG. 4.—Back-scattered electron micrographs from siderite concretions. A) General microstructure of the BH2 concretion. B) High-magnification view of zoned siderite crystallites from within the BH2 concretion. Note the late Fe-Mn-rich siderite (arrow) that overgrows the main body of the crystallite.
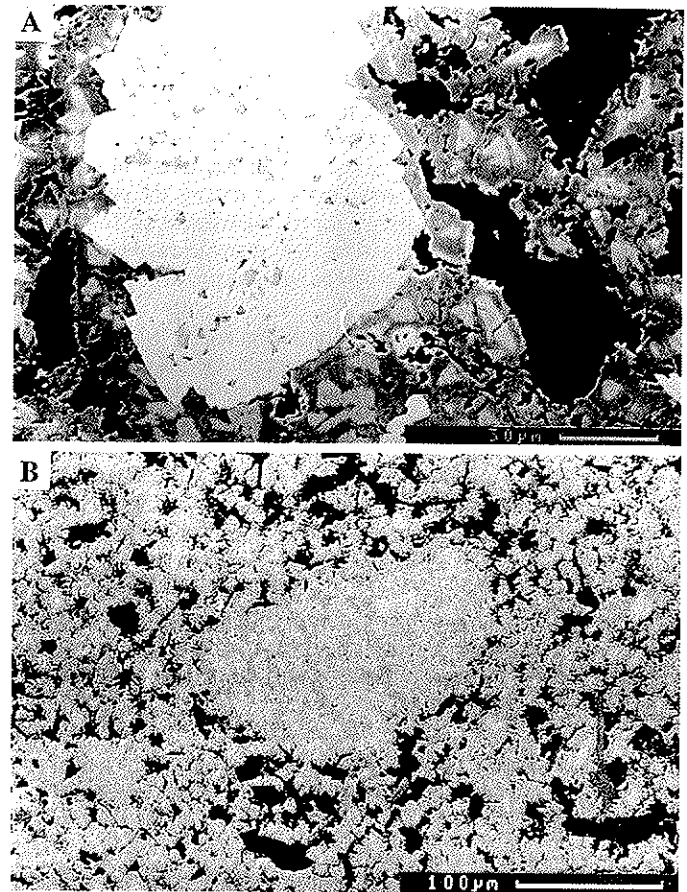
B). The main bodies of the siderite crystallites, described above, have been overgrown by two much thinner siderite zones; the first is Mn-rich and the second Mg-Ca-rich (Fig. 4B). The boundary between the bulk of the crystallite and overgrowths is sharper than the boundary between the inner zones. The thickness of the overgrowths is usually $\sim$ 1–2 μm, but in areas of the concretion where the crystallites are particularly densely packed the two outer zones are less prominent and are in some cases absent. It is interesting to note that these siderite crystallites have a morphology similar to those from the concretions in the Barrow Sandstone described by Mozley (1989). Apart from these few subtle variations, there is no difference in the size of the siderite crystallites, or the nature of their zoning, across either the BH2 or the BH4 concretions.

The siderite crystallites in the BH7 concretion are more equant than those described above and have a grain size of $\sim$ 10–25 μm (Fig. 5A). The crystallites exhibit conspicuous compositional zoning, superficially similar to that observed in the other concretions, i.e., Fe-Mn-rich siderite surrounded by a Mg-Ca-rich variety, but the boundary between these zones is far less diffuse (Fig. 5A). In some cases the siderite crystallites form subspherical aggregates up to 300 μm in diameter (Fig. 5B).

The BH5 concretion contains crystallites whose size and shape resemble those from BH7, but compositional zonation is very diffuse and individual crystallites do not appear to exhibit the full solid-solution range observed in the other concretions. In the BH5 and BH7 concretions, thin siderite overgrowths, as observed in the BH2 and BH4 concretions, are not present. No differences were observed in the size or nature of the zoning of the siderite crystallites across the BH5 and BH7 concretions.

FIG. 5.—Back-scattered electron micrographs of siderite concretions. A) Euhedral pyrite grain (very light region) surrounded by zoned siderite within the BH7 concretion. Note the siderite inclusions within the pyrite. B) Zoned siderite crystallites (light grains) from within the BH7 concretion. Note the large aggregate in the center of the frame. C) Organic matter (very dark areas) and micas (m) wrapped around siderite (s) crystallites in a sample taken from the edge of the BH2 concretion. Note that the siderite crystallites are far larger than the grain size of the detrital phases. The black regions on the micrographs A and B contain detrital grains and microporosity.

Siderite cement has not filled the microporosity between detrital grains, as previous models have implied (e.g., Curtis et al. 1986). Instead, it is present as very large crystallites that have displaced the surrounding detrital grains. This is well illustrated by the photomicrograph from the edge of the BH2 concretion (Fig. 5C); here the vast majority of pores do not contain

siderite, and where present the siderite crystallites are far larger than the individual pores within the sediment would have been. The siderite crystallites must have grown by either replacing, or more likely, displacing the surrounding detrital grains. Overall, the amount of siderite and number of crystallites per unit area decreases towards the outer margin of each concretion. However, this is not a regular decline; the density of crystallite packing is extremely heterogeneous, and even towards the edges of the concretions there are small regions of densely packed siderite. Towards the edges of the BH2 and BH4 concretions there is an increased tendency for the lath-shaped siderite crystallites to be oriented parallel to the bedding (e.g., Fig. 5C).

The grain size of detrital silicate phases differs greatly between the concretions. The average grain size of the silicates in the BH2 and BH4 concretions is probably between 2 μm and 5 μm, while the BH5 concretion contains grains between 5 μm and 10 μm, and the average for the BH7 concretion is $\sim$ 15 μm. The siderite crystallites are far larger than the detrital phases within these concretions. Only the silicate phases already detected by XRD were identified using BSEM/EDX analysis, i.e., quartz, kaolin, mica, and chlorite. In samples from the centers of concretions, micas show no strong preferred orientation, although in some cases they are bent around siderite crystallites. Towards the edges of concretions micas are frequently oriented parallel to the bedding and, along with organic debris, are in some cases wrapped around siderite crystallites (e.g., Fig. 5C).

EPMA Results.—The electron microprobe was used to trace chemical variations across individual siderite crystallites in each concretion, with analyses taken at 1 μm intervals (Fig. 6). The chemical trends across individual crystallites are similar to the bulk mineral-chemical trends across the individual concretions described above, i.e., the Fe/Mg, Fe/Ca, and Mn/Mg ratios decrease from the centers to the edges of crystallites. However, the local variation of chemical compositions across individual crystallites far exceeds the variation in bulk mineral chemistry that exists across concretions (compare Figure 3 and Figure 6).

The centers of crystallites from BH2 and BH4 show a pronounced enrichment in Mn (27 mole % in the center of a crystallite from BH4). Mn is also enriched in the centers of crystallites in the BH7 concretion (reaching 10 mole %), but not to the same extent as observed in BH2 and BH4. Mn reaches only $\sim$ 0.9 mole % in the siderite from the BH5 concretion, but a very slight enrichment towards the centers of the crystallites is still apparent. The Mn content of all crystallites examined is between 0.5 and 1.5 mole % at their margins. Mg is present in concentrations of less than 0.5 mole % in the centers of crystallites from the BH2, BH4, and BH7 concretions. On the other hand, the Mg content is $\sim$ 7 mole % in the centers of crystallites from the BH5 concretion. The Mg content increases towards the margins of all crystallites in all of the concretions, reaching upwards of 25 mole %. Calcium increases across crystallites in a manner similar to Mg, but the Ca content is between 2.5 and 4 mole % in their centers, which is far higher than Mg concentrations. The Ca content of most crystallites reaches a maximum of $\sim$ 10 mole % at their margins, which is far less than Mg concentrations. Consequently, there is an increase in the Mg/Ca ratio across the siderite crystallites. The same zonation was found in all crystallites examined from each concretion no matter if they were taken from their margins or centers.

The variation in the Fe content of crystallites is often more complicated because it is coupled to the changes in Mg, Mn, and to a lesser extent Ca. Fe concentrations tend to be relatively low (68 mole %) in the centers of crystallites in the BH2 and BH4 concretions (because of Mn enrichment) but begin to increase towards their margins as Mn decreases. A maximum Fe content (92 mole %) is reached before the effects of increasing Mg and Ca cause a decrease (58 mole %) in Fe towards the margins (e.g., Fig. 6A, B). The Fe profile in the siderite from the BH5 and BH7 concretions is slightly different: the central Mn enrichment is not sufficient to cause any noticeable depletion in Fe, so Fe concentrations are at a maximum in the centers of the crystallites and decrease gradually towards their margins (Fig. 6C, D).

Stable Carbon Isotope Results.—The results of the stable carbon isotopic study are given in Table 1. Siderite within subsamples from the edge of the BH2 concretion has δ^{13}C values as low as +0.8‰, whereas siderite within the subsamples taken from the center of this concretion has δ^{13}C values as high as +4.2‰. Siderite within subsamples from the edge of the BH4 concretion has δ^{13}C values as high as +4.8‰, whereas that from the center of this concretion has δ^{13}C values as high as +8.9‰. The carbon isotopic results in both concretions show the same overall trend, i.e., δ^{13}C decreases towards the edge of the concretion. Plots of δ^{13}C against Mg and of δ^{13}C against Mn for the siderite within the subsamples from the BH2 concretion are shown in Figures 7A and C, respectively. Equivalent plots for the siderite within the subsamples from the BH4 concretion are shown in Figures 7B and D, respectively. All plots reveal strong correlations, but those for the δ^{13}C–Mn data are not quite as strong as for the δ^{13}C–Mg data, probably because of the slightly higher errors associated with measuring the bulk Mn content within the siderite. The Mn data for both concretions had one outlier, therefore regressions have been calculated with and without this point for each concretion. These results are similar to those reported by Pearson (1979) and Curtis et al. (1986) and suggest mixing of phases with different δ^{13}C.

Extrapolation of the regression lines on the δ^{13}C–Mg plots to the siderite compositional values obtained by EPMA suggests that the early low-Mg siderite within the BH2 concretion has a δ^{13}C value of $\sim$ +13‰, whereas the later Mg-rich siderite has a δ^{13}C value of $\sim$ −5‰. The same calculations for the data from the BH4 concretion suggests the early low-Mg siderite has a δ^{13}C value of $\sim$ +10‰ and the later Mg-rich siderite has a δ^{13}C value of $\sim$ −1‰. Extrapolation of the results to the siderite compositional values obtained by EPMA produces δ^{13}C values of $\sim$ −10‰ and $\sim$ −0‰ for the low-Mn siderite in the BH2 and BH4 concretions, respectively, and values of $\sim$ +45‰ and $\sim$ +25‰ for the Mn-rich siderite in the BH2 and BH4 concretions, respectively. The extrapolations to the low-Mn siderite and the Mg-rich siderite are consistent and probably realistic. However, the values obtained by extrapolating the regressions to Mn-rich siderite produces δ^{13}C values that are higher than have been measured in nature. The reason for this is that carbonate with high δ^{13}C values is contained not only in the central zone of Mn-rich siderite but in the surrounding zone of Fe-rich siderite. In other words, the isotopic results are consistent with the siderite being composed of two end-member types, a Fe-Mn-rich variety with δ^{13}C values of $\sim$ +10‰ and a Mg-Ca-rich variety with δ^{13}C values of $\sim$ 0‰ to −5‰. Overall, it appears that the true range of δ^{13}C values of the siderite varies by around 5‰ either side of that measured by bulk-chemical analysis.

DISCUSSION

Implications of Electron Optical Studies for Growth Models

Previous models for the growth of the Hepworth siderite concretions have assumed that carbonate precipitated passively, filling all pore space. Estimates of porosity and burial depth at the time of siderite precipitation have been made on the basis of this assumption (e.g., Curtis et al. 1986). However, the large size of the siderite crystallites compared to the size of detrital phases within these concretions demonstrates that the siderite precipitated by either replacing or, more likely, displacing the surrounding detrital grains. Also, it has been shown that siderite did not fill all available pore space, indicating that the low proportion of carbonate cement at the edges of concretions cannot be interpreted as providing evidence that precipitation occurred during deep burial. These petrographic data clearly suggest that depth of precipitation cannot be estimated from the proportion of carbonate in the Hepworth siderite concretions, and a reevaluation of the processes responsible for the growth of the Hepworth concretions is required.
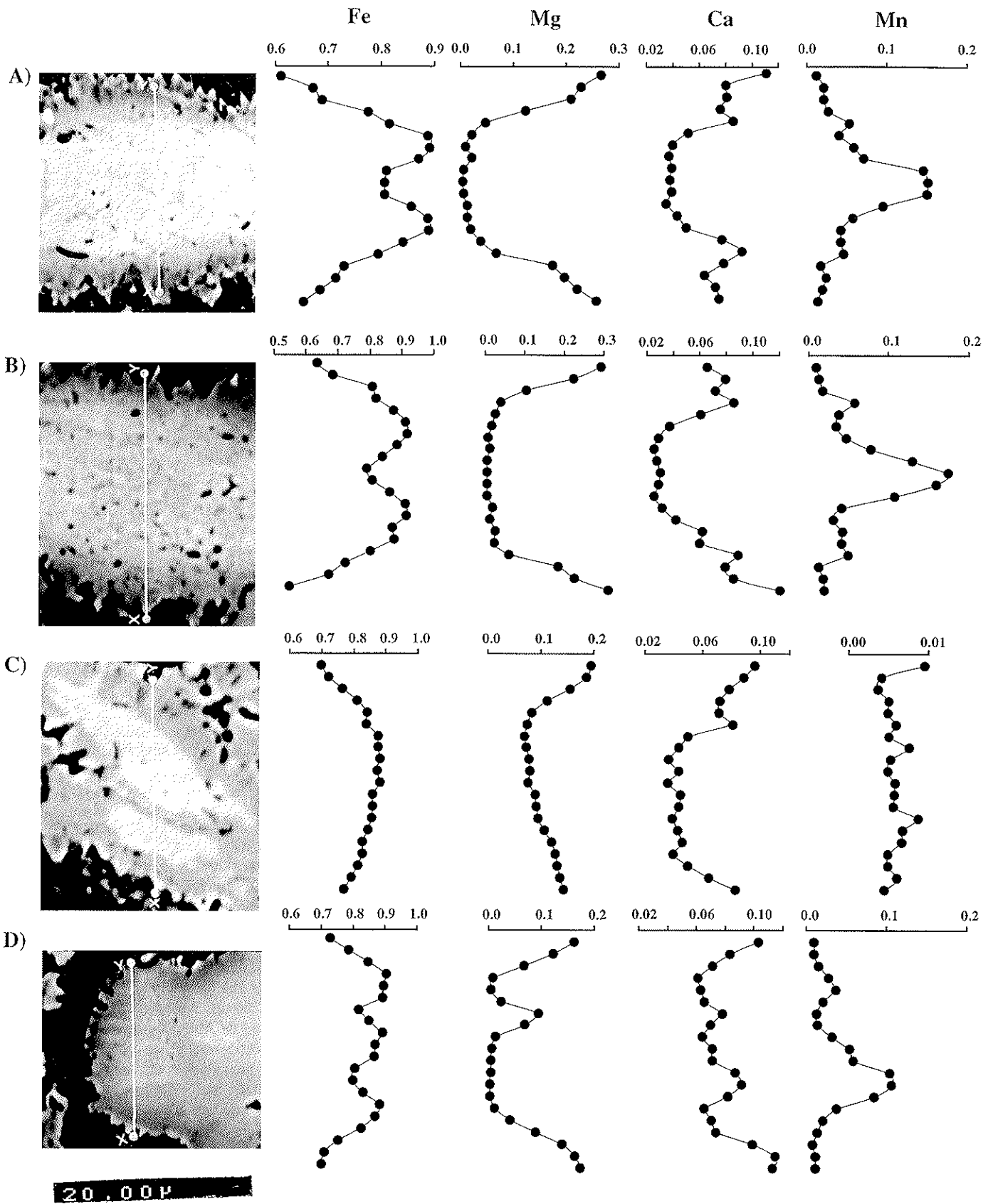
FIG. 6.—Chemical variations across individual crystallites within the A) BH2, B) BH4, C) BH5, and D) BH7 concretions determined by EMPA. The analyses were taken at ~ 1 μm intervals, and the results quoted are the fraction of end-member carbonate phase present.
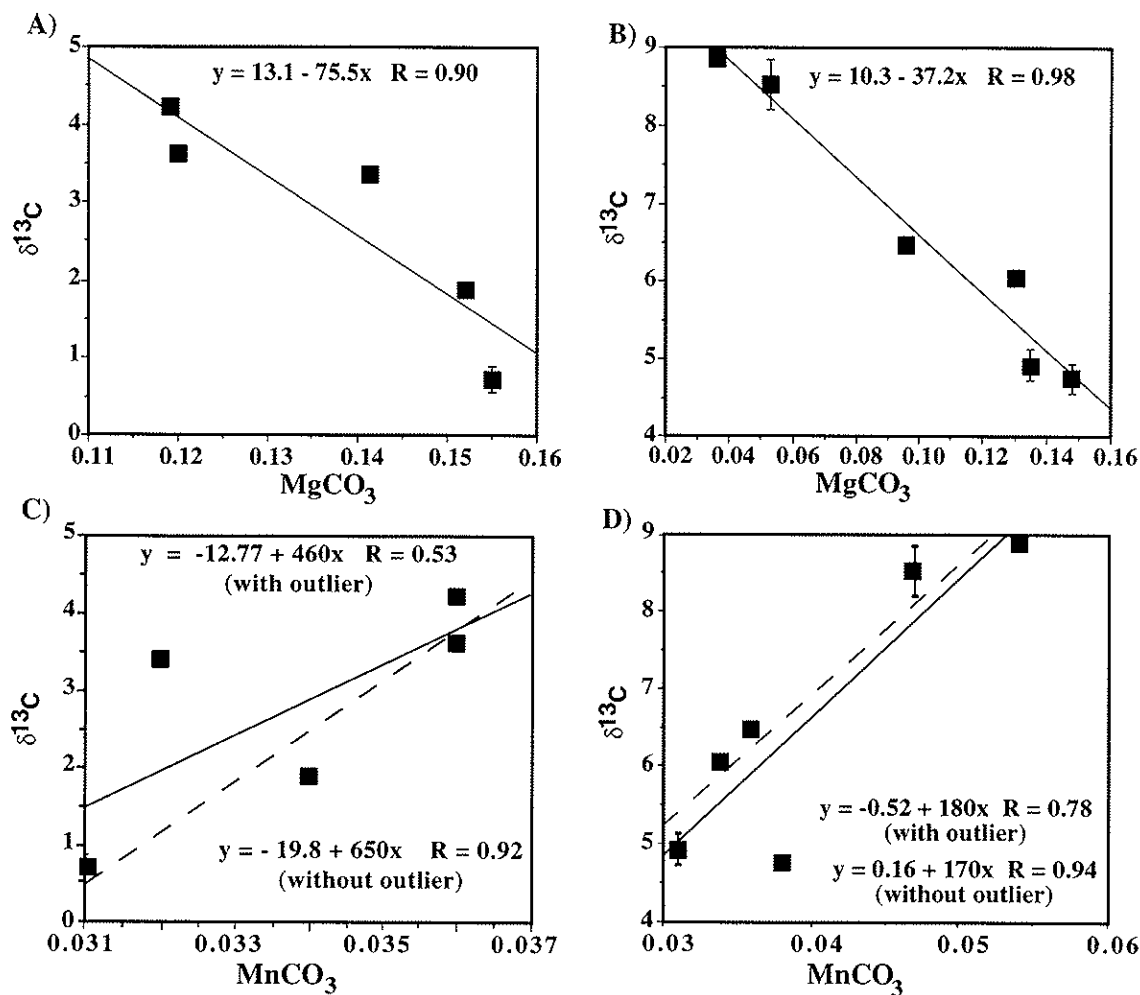
Fig. 7.—Plots of $\delta^{13}C$ against the proportion of end-member $MgCO_3$ within selected siderite subsamples from the A) BH2 and B) BH4 concretions, and $MnCO_3$ within the siderite from the C) BH2 concretion and D) BH4 concretion. The ranges on the points represent the standard deviations of the analyses conducted.

If the concretions had grown slowly from the center outwards during burial, the size and chemistry of the siderite crystallites would be expected to exhibit a systematic variation across individual concretions. In particular, it would be expected that the siderite crystallites in the centers of the concretions would be large compared to those at the margins which precipitated after sediment compaction. The observation that the siderite crystallites are strikingly similar across individual concretions is more consistent with their contemporaneous precipitation and with the decrease in the amount of carbonate across each concretion simply reflecting a decrease in the number of siderite crystallites. The quantity of siderite to precipitate at the edges of the concretions was clearly never limited by the amount of available pore space, as is implied by the porosity occlusion model of Curtis et al. (1986).

Oertel and Curtis (1972) presented XRD work which showed that kaolinite in the centers of the concretions is essentially randomly oriented while that at the edges of concretions is aligned parallel to the bedding. These results were taken as evidence that concretions grew from the center outwards and that the siderite precipitated by passively replacing all available pore space during burial. The petrographic data presented above suggest that a more likely interpretation of the X-ray data is that the lower proportion of siderite at the edges of the concretions allowed the kaolinite to be reoriented during compaction. The large proportion of siderite in the

centers of the concretions prevented the kaolinite from being reoriented during compaction.

Since the siderite crystallites appear virtually identical, both in chemistry and morphology, everywhere within an individual concretion, it is not initially obvious why bulk chemical variations across the concretions exist. It was noted earlier, however, that the siderite overgrowths vary in thickness depending on the density of crystallite packing. It seems likely that the Mg-Ca-rich siderite also shows a similar distribution. A simple calculation based on the EPMA data indicates that the outer third of each crystallite in the BH2 and BH4 concretions contains approximately 98% of the Mg, and 90% of the Ca but only 25% of the Mn of the crystallite as a whole. The small bulk chemical variations across concretions could therefore result from very subtle variations in the proportion of the later Mg-Ca-rich siderite to the earlier Fe-Mn-rich variety. Such differences need only be extremely small to produce the reported bulk chemical variations and are unlikely to be detectable using BSEM. For example, a 5% difference in the ratio of the Mg-Ca-rich to Fe-Mn-rich siderite across the BH2 concretion can account for the bulk chemical variations observed.

In terms of the growth history, the BSEM results suggest that Mn-rich siderite nuclei precipitated throughout the concretion at approximately the same time. The change in pore-water composition during the siderite precipitation is therefore reflected more precisely by the variation in the chem-

istry of individual crystallites than by the bulk changes in the chemistry across the concretions.

The zoned nature of the crystallites also has implications for the interpretation of bulk chemical and isotopic data, namely, any bulk composition is merely the average of a whole chemical and isotopic continuum and the full degree of isotopic variation may have been severely subdued (Feistner 1989).

Major-Cation Chemistry of Siderite

Curtis et al. (1986) suggested that Mn-siderite, such as that present in cores of siderite crystallites within the BH2 and BH4 concretions, precipitated close to the sediment–water interface, the Mn and Fe being supplied by reduction of manganese and ferric oxides. This explanation is consistent with results of modern pore-water studies of both marine (Froelich et al. 1979; Sørensen and Jørgensen 1987; Sholkovitz et al. 1989) and nonmarine environments (Robbins and Callender 1975; Emerson 1976), which show that pore waters may become greatly enriched in Mn at very shallow depths (< 0.5 m below sediment–water interface). In all concretions analyzed, the Mn/Fe ratio decreases towards the edges of siderite crystallites. Curtis et al. (1986) pointed out that the decrease in Mn/Fe ratios across concretions is analogous with the results of modern pore-water studies, which have established that the concentration of Fe^{2+} frequently reaches a maximum somewhat deeper than Mn^{2+} (e.g., Emerson 1976; Froelich et al. 1979; Aller et al. 1986; Shaw et al. 1990; Carignan and Lean 1991).

The siderite within the BH5 and BH7 concretions is far less enriched in Mn than in the other concretions. Curtis et al. (1986) termed this "late" siderite and suggested that it formed after the Mn-rich variety when Mn reduction was not so active. However, "late" need not imply "at great depth" because manganese reduction is usually very active only close to the sediment–water interface.

Mg and Ca concentrations increase towards the margins of the siderite crystallites within all of the concretions studied, although this general pattern is complicated by the growth of late Mn-rich overgrowths. The exact controls on Mg and Ca substitution within siderite are poorly understood (e.g., rate of precipitation, Mg/Fe and Ca/Fe ratios, salinity, etc.). However, it seems likely that increases in the ratio of Mg and Ca to Fe within pore waters would cause an increase in the Mg and Ca substitution within siderite (Curtis et al. 1986).

The source of the Mg and Ca within the siderite from the Hepworth concretions remains problematic. Pearson (1979 and 1985) favored release of Mg by clay-mineral reaction. On the other hand, Curtis et al. (1986) suggested that the overlying water column is a possible source of Mg and Ca. Studies of modern sediments undergoing active siderite precipitation have shown the Mg/Fe ratio of pore water may increase with depth very close (within 3 m) to the sediment–water interface. For example, dissolved Fe and Mn within the pore waters from sediments on the Amazon Shelf decrease rapidly after their maximum concentrations are reached (at ~ 20 cm and 50 cm below the sediment–water interface, respectively; Aller et al. 1986). However, Ca and Mg concentrations remain constant with depth, so at depths greater than ~ 50 cm below the sediment–water interface the Mg/Fe and Ca/Fe ratios increase. The increase in Mg/Fe and Ca/Fe ratios within these pore waters is probably caused by precipitation of siderite combined with a decrease in the rate of iron reduction with depth, as the most labile organic matter (e.g., Berner 1980; Middelburg 1989) and iron minerals (e.g., Canfield 1989) become depleted with time.

It is therefore apparent that the depth-related changes in the Fe, Mn, Ca, and Mg content of the pore waters within recently deposited sediments resemble the chemical variations across individual siderite crystallites reported in this study. Several lines of evidence suggest that processes that occurred close to the sediment–water interface were far more important in the formation of the Mg-Ca-rich siderite than the deeper processes favored by other workers (e.g., Pearson 1979, 1985; Curtis and Coleman 1986;

Curtis et al. 1986). First, the BSEM study revealed that Mg-Ca-rich siderite is well developed in the centers of the concretions, which suggests that it precipitated before significant compaction. Second, the late Mn-rich overgrowths within the BH2 and BH4 concretions (Fig. 4B) suggest that the pore waters experienced a decrease in Mg/(Fe + Mn) and Ca/(Fe + Mg) ratios late in their growth history. This is easily explained by early diagenetic processes, such as diffusion of Fe and Mn from freshly deposited sediments undergoing rapid rates of iron and manganese reduction. However, there is no obvious reason why the concentrations of Mn and Fe within pore waters should suddenly increase as a result of deep burial reactions. Third, the $^{87}Sr/^{86}Sr$ ratio of the siderite (0.7094 to 0.7104) is indistinguishable from that of the francolite, which is unequivocally an early diagenetic precipitate (Fisher 1992). Fourth, the clay-mineral assemblage within these sediments appears to be composed of essentially detrital minerals; analytical transmission electron microscopic (ATEM) analysis failed to find any evidence of illite authigenesis, suggesting that smectite-to-illite transformation did not supply Mg and Ca for siderite precipitation (Fisher 1992).

$\delta^{13}C$ Variations across Sideritic Concretions

The carbon-isotope data presented above show that the $\delta^{13}C$ value of the siderite decreases with increasing Mg substitution. These results are in agreement with $\delta^{13}C$ measurements made on sideritic concretions from this area in other studies (e.g., Curtis et al. 1975; Pearson 1979; Curtis and Coleman 1986; Curtis et al. 1986). Pearson (1979) suggested that the $\delta^{13}C$ variations result from mixing of two distinct carbonate phases, a pure siderite that has a very positive $\delta^{13}C$ composition and a pistomesite (Mg-rich siderite), which has a negative $\delta^{13}C$ signature. The electron optical results have clearly shown that, instead of two distinct iron carbonate phases, each concretion contains a single phase of compositionally zoned siderite whose central regions have $\delta^{13}C$ compositions in excess of $+10‰$, and whose outer Mg-Ca-rich regions have $\delta^{13}C$ as low as ~ $-5‰$.

Previous studies have proposed that carbonate within the siderite was derived principally from two sources: methanogenic reactions produced carbonate with positive $\delta^{13}C$, while the carbonate with negative $\delta^{13}C$ was produced by thermal decarboxylation (Pearson 1979; Curtis et al. 1986). The decrease in the $\delta^{13}C$ value across the concretions was attributed to the increased importance of thermal decarboxylation as both burial and concretionary growth progressed. There is certainly a strong justification for implying that methanogenic reactions supplied the early carbonate with positive $\delta^{13}C$, namely, methanogenesis is the dominant organic-matter oxidizing process in all locations where dissolved inorganic carbon (DIC) with $\delta^{13}C > +5‰$ has been reported from interstitial fluids of modern siliciclastic sediments (e.g., Nissembaum et al. 1972; Claypool and Kaplan 1974; LaZerte 1981; Turner and Fritz 1983; Kuivila and Murray 1984; Whiticar et al. 1986; Herczeg 1988). However, without the support of porosity estimates derived from the proportion of carbonate within the concretions, there seems to be no compelling evidence in favor of thermal decarboxylation being the source of the later carbonate with negative $\delta^{13}C$. For this reason the controls on the $\delta^{13}C$ composition of DIC within methane producing sediments is discussed below.

The $\delta^{13}C$ Composition of DIC in Methane-Producing Sediments

It has become commonplace to interpret carbonates with positive $\delta^{13}C$ compositions as products of methanogenesis, and carbonate with negative values as being produced by other processes such as sulfate reduction or decarboxylation. However, many studies have measured the isotopic composition of dissolved inorganic carbon (DIC) within methane-producing sediments, and the results show enormous variation ($\delta^{13}C$ values ranging between -30 and $+20‰$; Whiticar et al. 1986). Only a very small number of sediments are known that contain DIC with a positive $\delta^{13}C$ composition

(Turner and Fritz 1983; Whiticar et al. 1986). In other words, DIC with positive $\delta^{13}C$ is the exception rather than the rule in methanogenic environments. Not only does the $\delta^{13}C$ composition of DIC within methanogenic sediments vary between locations, there is some evidence to suggest that it may vary during sediment burial. For example, Turner and Fritz (1983) presented a depth profile of $\delta^{13}C_{DIC}$ within methane-producing sediments deposited in a freshwater lake, with $\delta^{13}C_{DIC}$ first increasing with depth to a maximum (at ~ 3 m below the sediment–water interface), then decreasing towards the bottom of the core.

It is uncertain why $\delta^{13}C_{DIC}$ would become more negative with depth in a methanogenic environment, because methanogenesis is a very poorly understood, complex multistage process. However, there seems no reason why the variation in the isotopic composition of the siderite examined during this study could not have resulted from processes acting close to the sediment–water interface in a methanogenic environment. Therefore the fact that the $\delta^{13}C$ value of the siderite became more negative as it precipitated does not place any constraints upon the depth to which precipitation continued. Furthermore, the $\delta^{13}C$ value of the siderite does not conflict with the suggestion presented in this paper that concretion growth may have entirely occurred close to the sediment–water interface.

CONCLUSIONS

The siderite concretions from the Hepworth quarries are composed of 50–100 μm compositionally zoned crystallites. The centers of these crystallites tend to be enriched in Fe and Mn whereas their margins are Mg-Ca-rich. The bulk mineral chemistry of the siderite across concretions varies far less than composition across individual crystallites. The shape distribution and size of the crystallites indicate that they did not grow by passive replacement of all available pore space. Instead, they displaced detrital grains and did not fill all available pore space. These observations have three major implications for the growth of the Hepworth siderite concretions:

(1) The proportion of siderite within any part of the concretion cannot be used to calculate the porosity of the host sediment at the time of cement precipitation.

(2) Bulk analysis even of centripetal samples does not provide precise information as to the chemical or isotopic composition of discrete phases of siderite precipitate. Instead, it provides the average composition of several zones of siderite cement.

(3) The siderite concretions do not appear to have grown progressively from the center outwards as previous models have implied. Instead, individual nuclei grew throughout the volume of the concretion at approximately the same time and further carbonate precipitation continued by growth of these crystallites.

Without support from porosity estimates there seems little justification for implying that deep burial processes contributed solutes for precipitation of the later Mg-Ca-rich siderite. Instead, it is proposed that concretions started to grow close to the sediment–water interface, where rates of iron reduction, CO_2 reduction, and in some cases manganese reduction were high. This siderite is often enriched in Mn, with only minor Mg substitution, and has a very positive $\delta^{13}C$ composition. As organic matter and ferric/manganese oxides were depleted, rates of iron reduction, manganese reduction, and CO_2 reduction fell, increasing the Ca/Fe and Mg/Fe ratio of the pore waters, the Ca and Mg being supplied from the overlying water column. As the rate of CO_2 reduction decreased, other sources of carbonate became more important; these had lower carbon isotopic compositions, resulting in a decrease in the $\delta^{13}C$ value of the precipitating siderite. Although the exact sources of the lighter carbonate have not been unequivocally established, it is clear that it could be generated within methanogenic sediments without the need to infer deeper burial processes such as thermal decarboxylation.

Bulk chemical and isotopic variations in the composition of siderite

across and between concretions cannot be used to justify a general zonal scheme for shale diagenesis.

REFERENCES

ALLER, R.C., MACKIN, J.E., AND COX, R.T., JR., 1986, Diagenesis of Fe and S in Amazon inner shelf muds: Apparent dominance of Fe reduction and implications for the genesis of ironstones: Continental Shelf Research, v. 6, p. 263–289.

BALDWIN, B., AND BUTLER, C.O., 1985, Compaction curves: American Association of Petroleum Geologists, Bulletin, v. 69, p. 622–626.

BERNER, R.A., 1980, Early Diagenesis: A Theoretical Approach: Princeton, New Jersey, Princeton University Press, 241 p.

CALVER, M.A., 1968a, Distribution of Westphalian marine faunas in northern England and adjoining areas: Yorkshire Geological Society, Proceedings, v. 37, p. 1–72.

CALVER, M.A., 1968b, Coal Measures invertebrate faunas, in Murchison, D., and Westoll, T.S., eds., Coal and Coal-Bearing Strata: Edinburgh and London, Oliver & Boyd, p. 147–175.

CANFIELD, D.E., 1989, Reactive iron minerals in sediments: Geochimica et Cosmochimica Acta, v. 53, p. 619–632.

CARIGNAN, R., AND LEAN, D.R.S., 1991, Regeneration of dissolved substances in a seasonally anoxic lake: The relative importance of processes occurring in the water column and in the sediments: Limnology and Oceanography, v. 36, p. 683–707.

CLAYPOOL, G.E., AND KAPLAN, I.R., 1974, The origin and distribution of methane in marine sediments, in Kaplan, I.R., ed., Natural Gases in Marine Sediments: New York, Plenum Press, p. 99–139.

COLEMAN, M.L., AND RAISWELL, R., 1993, Microbial mineralisation of organic matter: mechanisms of self-organisation and inferred rates of precipitation of diagenetic minerals: Royal Society [London], Philosophical Transactions, v. A344, p. 69–87.

CURTIS, C.D., 1977, Sedimentary geochemistry: environments and processes dominated by involvement of an aqueous phase: Royal Society [London], Philosophical Transactions, v. A286, p. 353–372.

CURTIS, C.D., AND COLEMAN, M.L., 1986, Controls on the precipitation of early diagenetic calcite, dolomite and siderite concretions in complex depositional sequences, in Gautier, D.L., ed., Roles of Organic Matter during Diagenesis: SEPM, Special Publication 38, p. 23–33.

CURTIS, C.D., COLEMAN, M.L., AND LOVE, L.G., 1986, Pore water evolution during sediment burial from isotopic and mineral chemistry of calcite, dolomite and siderite concretions: Geochimica et Cosmochimica Acta, v. 50, p. 2321–2334.

CURTIS, C.D., PEARSON, M.J., AND SOMOGYI, V.A., 1975, Mineralogy, chemistry and origin of a concretionary siderite sheet (clay-ironstone band) in the Westphalian of Yorkshire: Mineralogical Magazine, v. 40, p. 385–93.

EMERSON, S., 1976, Early diagenesis in anaerobic lake sediments: chemical equilibria in interstitial waters: Geochimica et Cosmochimica Acta, v. 40, p. 925–934.

FEISTNER, K.W.A., 1989, Petrographic examination and re-interpretation of concretionary carbonate horizons from the Kimmeridge Clay, Dorset: Geological Society of London, Journal, v. 146, p. 345–350.

FISHER, Q.J., 1992, Geochemical and isotopic investigations of diagenesis in the Hepworth Sequence (Westphalian), Northern England [unpublished Ph.D. thesis]: University of Leeds, 241 p.

FROELICH, P.N., KLINKHAMMER, G.P., BENDER, M.L., LUEDTKE, N.A., HEATH, G.R., CULLEN, D., DAUPHIN, P., HAMMOND, D., HARTMAN, B., AND MAYNARD, V., 1979, Early oxidation of organic matter in pelagic sediments of the eastern equatorial Atlantic: suboxic diagenesis: Geochimica et Cosmochimica Acta, v. 43, p. 1075–1090.

GAUTIER, D.L., AND CLAYPOOL, G.E., 1984, Interpretation of methanogenic diagenesis in ancient sediments by analogy with processes in modern diagenetic environments, in McDonald, D.A., and Surdam, R.C., eds., Clastic Diagenesis: American Association of Petroleum Geologists, Memoir 37, p. 111–123.

HERCZEG, A.L., 1988, Early diagenesis of organic matter in lake sediments: A stable carbon isotopic study of pore waters: Chemical Geology, v. 72, p. 199–209.

HOWER, J., ESLINGER, E.V., HOWER, M.E., AND PERRY, E.A., 1976, Mechanism of burial metamorphism in argillaceous sediment: 1. Mineralogical and chemical evidence: Geological Society of America, Bulletin, v. 87, p. 725–737.

IRWIN, H., COLEMAN, M.L., AND CURTIS, C.D., 1977, Isotopic evidence for the source of diagenetic carbonates formed during burial of organic-rich sediments: Nature, v. 269, p. 209–213.

KUIVILA, K.M., AND MURRAY, J.W., 1984, Organic matter diagenesis in freshwater sediments: The alkalinity and total CO_2 balance and methane production in the sediments of Lake Washington: Limnology and Oceanography, v. 29, p. 1218–1230.

LAZERTE, B.D., 1981, The relationship between total dissolved carbon dioxide and its stable

carbon isotopic composition in aquatic sediments: Geochimica et Cosmochimica Acta, v. 45, p. 647–656.

LIPPMANN, F., 1955, Ton, Geoden und Minerale des Barreme von Hoheneggelsen: Geologische Rundschau, v. 43, p. 475–503.

MIDDELBURG, J.J., 1989, A simple rate model for organic matter decomposition in marine sediments: Geochimica et Cosmochimica Acta, v. 53, p. 1577–1581.

MORTIMER, R.J.G., AND COLEMAN, M.L., 1997, Microbial influence on the oxygen isotopic composition of diagenetic siderite: Geochimica et Cosmochimica Acta, v. 61, p. 1705–1711.

MOZLEY, P.S., 1989, Complex compositional zonation in concretionary siderite: implications for geochemical studies: Journal of Sedimentary Petrology, v. 59, p. 815–818.

MOZLEY, P.S., 1996, The internal structure of carbonate concretions in mudrocks: a critical evaluation of the concentric model of concretion growth: Sedimentary Geology, v. 103, p. 85–91.

NISSENBAUM, A., PRESLEY, B.J., AND KAPLAN, I.R., 1972, Early diagenesis in a reducing fjord, Saanich Inlet, British Columbia—I. Chemical and isotopic changes in major components of interstitial water: Geochimica et Cosmochimica Acta, v. 32, p. 1037–1048.

OERTEL, C., AND CURTIS, C.D., 1972, Clay-ironstone concretion preserving fabrics due to progressive compaction: Geological Society of America, Bulletin, v. 83, p. 2597–2606.

PEARSON, M.J., 1973, The geochemistry of a Westphalian sediment sequence [unpublished Ph.D. thesis]: University of Sheffield, 194 p.

PEARSON, M.J., 1974a, Siderite concretions from the Westphalian of Yorkshire: a chemical investigation of the carbonate phase: Mineralogical Magazine, v. 39, p. 696–699.

PEARSON, M.J., 1974b, Magnesian siderite in carbonate concretions from argillaceous sediments in the Westphalian of Yorkshire: Mineralogical Magazine, v. 39, p. 700–704.

PEARSON, M.J., 1977, Francolite in a concretion from argillaceous sediments in the Westphalian of Yorkshire: Mineralogical Magazine, v. 41, p. M4–M6.

PEARSON, M.J., 1979, Geochemistry of the Hepworth Carboniferous sediment sequence and the origin of the diagenetic iron minerals and concretions: Geochimica et Cosmochimica Acta, v. 43, p. 927–941.

PEARSON, M.J., 1985, Some chemical aspects of diagenetic concretions from the Westphalian of Yorkshire, England: Chemical Geology, v. 48, p. 231–241.

RAISWELL, R., 1971, The growth of Cambrian and Liassic concretions: Sedimentology, v. 17, p. 147–171.

ROBBINS, J.A., AND CALLENDER, E., 1975, Diagenesis of manganese in Lake Michigan sediments: American Journal of Science, v. 275, p. 512–533.

ROSENFELD, W.D., AND SILVERMAN, S.R., 1959, Carbon isotopic fractionation in bacterial production of methane: Science, v. 130, p. 1658–1659.

SEIBOLD, E., 1962, Kalk-Konkretionen und karbonatisch gebundenes Magnesium: Geochimica et Cosmochimica Acta, v. 26, p. 899–909.

SHAW, T.J., GIESKES, J.M., AND JAHNKE, R.A., 1990, Early diagenesis in differing depositional environments: The response of transition metals in pore water: Geochimica et Cosmochimica Acta, v. 54, p. 1233–1246.

SHOLKOVITZ, E.R., PIEPGRAS, D.J., AND JACOBSEN, S.B., 1989, The pore water chemistry of rare earth elements in Buzzards Bay sediments: Geochimica et Cosmochimica Acta, v. 53, p. 2847–2856.

SØRENSEN, J., AND JØRGENSEN, B.B., 1987, Early diagenesis in sediments from the Danish coastal waters: microbial activity and Mn–Fe–S geochemistry: Geochimica et Cosmochimica Acta, v. 51, p. 1583–1590.

TURNER, J.V., AND FRITZ, P., 1983, Enriched ^{13}C composition of interstitial waters in sediments of a freshwater lake: Canadian Journal of Earth Sciences, v. 20, p. 616–621.

WHITICAR, M.J., FABER, E., AND SCHOELL, M., 1986, Biogenic methane formation in marine and freshwater environments: CO_2 reduction vs. acetate fermentation—Isotopic evidence: Geochimica et Cosmochimica Acta, v. 50, p. 693–709.